Convergent evolution of zoonotic Brucella species toward the selective use of the pentose phosphate pathway

Machelart, Arnaud; Willemart, Kevin; Zúñiga-Ripa, Amaia; Godard, Thibault; Plovier, Hubert; Wittmann, Christoph; Moriyón, Ignacio; De Bolle, Xavier; Van Schaftingen, Emile; Letesson, Jean-Jacques; Barbier, Thibault

Published in:
Proceedings of the National Academy of Sciences of the United States of America

DOI:
10.1073/pnas.2008939117

Publication date:
2020

Document Version
Publisher's PDF, also known as Version of record

Convergent evolution of zoonotic *Brucella* species toward the selective use of the pentose phosphate pathway

Arnaud Machelart[a,b,1], Kevin Willemart[a,1], Amaia Zúñiga-Ripa[c], Thibault Godard[d], Hubert Plovier[e], Christoph Wittmann[f], Ignacio Moriyón[c], Xavier De Bolle[a,2], Emile Van Schaftingen[g,h], Jean-Jacques Letesson[a,3], and Thibault Barbier[a,i,2,3]

[a]Research Unit in Biology of Microorganisms, Narilis, University of Namur, B-5000 Namur, Belgium; [b]Center for Infection and Immunity of Lille, Université de Lille, CNRS, INSERM, Centre Hospitalier Universitaire de Lille, Institut Pasteur de Lille, U1019, Unité Mixtes de Recherche 9017, 59000 Lille, France; [c]Departamento de Microbiología e Instituto de Salud Tropical, Instituto de Investigación Sanitaria de Navarra, Universidad de Navarra, 31009 Pamplona, Spain; [d]Institute of Biochemical Engineering, Technische Universität Braunschweig, 38106 Braunschweig, Germany; [e]Metabolism and Nutrition Research Group, Louvain Drug Research Institute, Walloon Excellence in Life Sciences and Biotechnology (WELBIO), Université Catholique de Louvain (UCLouvain), 1200 Brussels, Belgium; [f]Institute of Systems Biotechnology, Universität des Saarlandes, 66123 Saarbrücken, Germany; [g]De Duve Institute, UCLouvain, 1200 Brussels, Belgium; [h]WELBIO, UCLouvain, 1200 Brussels, Belgium; and [i]Department of Immunology and Infectious Diseases, Harvard T. H. Chan School of Public Health, Boston, MA 02115

Edited by Roy Curtiss III, University of Florida, Gainesville, FL, and approved August 25, 2020 (received for review May 5, 2020)

Mechanistic understanding of the factors that govern host tropism remains incompletely understood for most pathogens. *Brucella* species, which are capable of infecting a wide range of hosts, offer a useful avenue to address this question. We hypothesized that metabolic fine-tuning to intrahost niches is likely an underappreciated axis underlying pathogens' ability to infect new hosts and tropism. In this work, we compared the central metabolism of seven *Brucella* species by stable isotopic labeling and genetics. We identified two functionally distinct groups, one overlapping with the classical zoonotic species of domestic livestock that exclusively use the pentose phosphate pathway (PPP) for hexose catabolism, whereas species from the second group use mostly the Entner–Doudoroff pathway (EDP). We demonstrated that the metabolic dichotomy among *Brucellae* emerged after the acquisition of two independent EDP-inactivating mutations in all classical zoonotic species. We then examined the pathogenicity of key metabolic mutants in mice and confirmed that this trait is tied to virulence. Altogether, our data are consistent with the hypothesis that the PPP has been incrementally selected over the EDP in parallel to *Brucella* adaptation to domestic livestock.

Brucella | metabolism | evolution | α-Proteobacteria

Mechanistic understanding of the factors that govern host adaptations remains elusive for most pathogens. To investigate this central question, Rhizobiales are of particular interest since they form an ecologically diversified bacterial order. They include free-living organisms (e.g., *Ochrobactrum* and *Caulobacter* spp.) as well as bacteria involved in different symbiotic relationships with eukaryotes, such as plant symbionts (*Rhizobium* spp.) or pathogens (*Agrobacterium* spp.) and animal pathogens (1). Among the latter, *Brucella* species are capable of infecting a broad range of vertebrates and cause a widespread zoonosis known as brucellosis (2, 3). Although other brucellae can cause human infections sporadically (4), human brucellosis is typically caused by species infecting domestic livestock (*Brucella abortus*, *Brucella melitensis*, *Brucella suis*; biovars [bv.] 1, 3, and 4; here, coined as classical zoonotic brucellae) and to a lesser extent by *Brucella canis* (5). Most *Brucella* species seem to have emerged through explosive irradiation as they form a core group separated from early branching species, like *Brucella inopinata*, which itself is closer to soil-living Rhizobiales (6). *Brucella* thus represent a remarkable model to investigate what makes a pathogen successful in comparison with its phylogenetic neighbors and the adaptations involved.

We hypothesized that metabolism fine-tuning to each niche is likely crucial. Based on genome sequences, the central metabolic network should similar in all *Brucella* species (7) and other Rhizobiales (8, 9). It includes all enzymes of the pentose phosphate pathway (PPP), Entner–Doudoroff pathway (EDP), Krebs cycle (tricarboxylic acid cycle), and glyoxylate shunt (7–9) but lacks classical glycolysis (Embden–Meyerhof–Parnas pathway [EMP]) because of the absence of 6-phosphofructokinase (Pfk) (see Fig. 1*A* for metabolic interactions between PPP, EDP, and EMP) (7, 10). Despite these similarities, the glucose catabolism of three classical *Brucella* species was shown to rely exclusively on the PPP for glucose catabolism (7, 11, 12), whereas *Rhizobium*, *Agrobacterium*, and *Caulobacter* species were experimentally shown to exploit the EDP instead (8, 9, 13). The prominent use of the PPP could, therefore, be a specific feature of the pathogenic *Brucella* and may represent an important step in their adaptation to the chemical landscape of the host.

Significance

***Brucella* species are capable of infecting a range of mammals, including humans, with relative host specificity. We hypothesized that metabolism is instrumental in host adaptation and compared the central metabolism of seven species. We demonstrate the existence of two distinct groups, including one overlapping with the classical zoonotic brucellae of domestic livestock that exclusively use the pentose phosphate pathway. Species from the second group rely mostly on the Entner–Doudoroff pathway instead. This metabolic dichotomy arose after the acquisition of two newly identified EDP-inactivating mutations. This selected trait seems to be linked to bacterial pathogenicity in mice. The data fit the hypothesis that *Brucella* has undergone a stepwise metabolic evolution in domestic hosts that might also apply to other pathogens.**

Author contributions: J.-J.L. and T.B. designed research; A.M., K.W., A.Z.-R., T.G., H.P., and T.B. performed research; A.M., K.W., A.Z.-R., T.G., H.P., C.W., I.M., X.D.B., E.V.S., J.-J.L., and T.B. analyzed data; and A.M., I.M., X.D.B., E.V.S., J.-J.L., and T.B. wrote the paper.

The authors declare no competing interest.

This article is a PNAS Direct Submission.

[1]A.M. and K.W. contributed equally to this work.

[2]To whom correspondence may be addressed. Email: xavier.debolle@unamur.be or thibault.barbier@outlook.com.

[3]J.-J.L. and T.B. contributed equally to this work.

This article contains supporting information online at https://www.pnas.org/lookup/suppl/doi:10.1073/pnas.2008939117/-/DCSupplemental.

First published October 5, 2020.

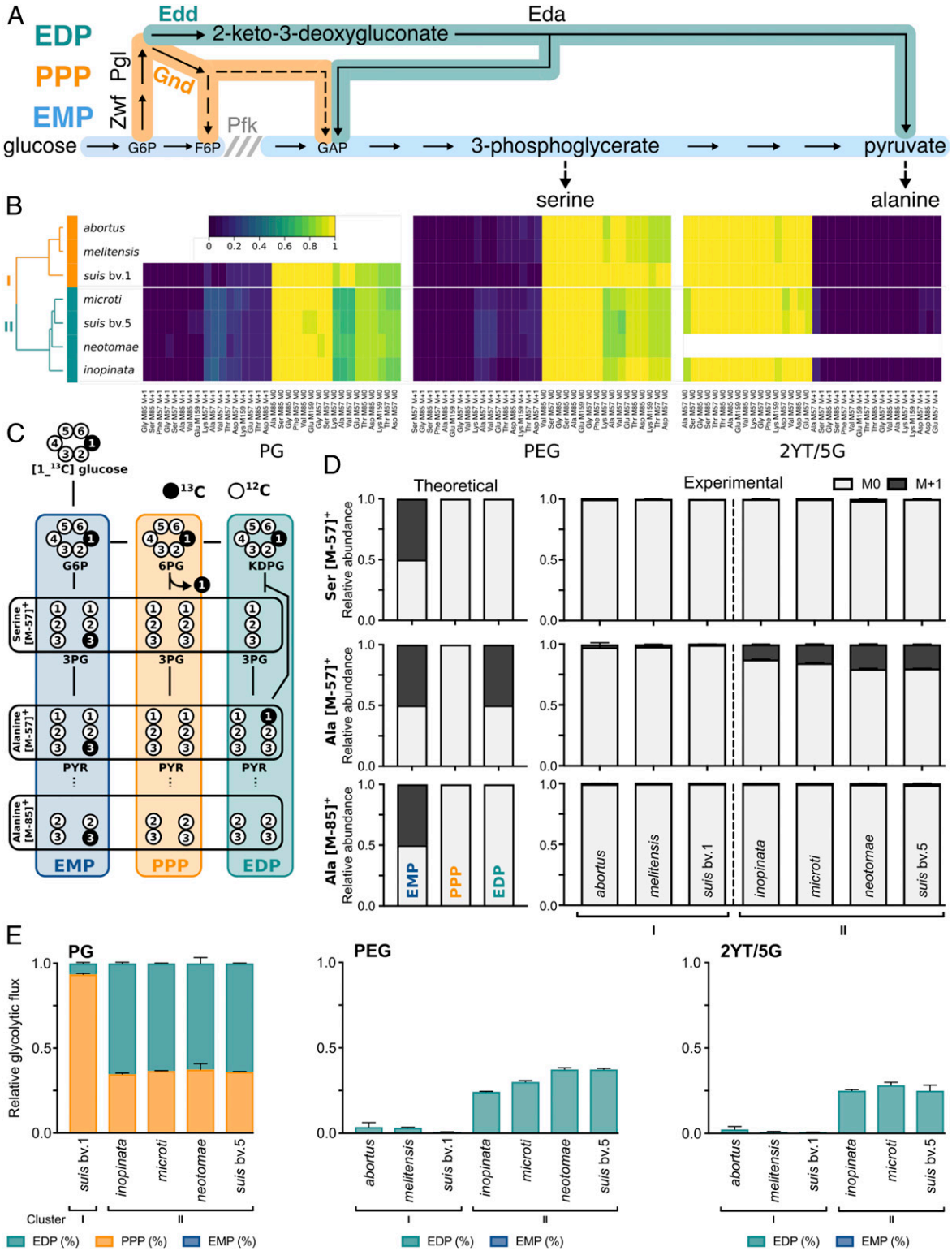

Fig. 1. Central metabolism characterization of seven *Brucella* species by isotope profiling. (*A*) Simplified view of the metabolic interactions between the EMP, EDP, and PPP. (*B*) Heat map representing the relative abundance of M0 and M + 1 fragments of isotopically labeled amino acids for seven *Brucella* species in three different media (PG, PEG, and 2YT/5G). (*C*) Carbon fate map of [1-^{13}C]glucose catabolized via glycolysis (blue), PPP (orange), or EDP (green). (*D*) Theoretical serine- and alanine-labeling patterns resulting from each glycolytic pathway (*Left*) and observed patterns for tested *Brucella* species (*Right*). (*E*) Estimations of pyruvate-synthesis fluxes via the different catabolic pathways. PPP contribution for glucose assimilation resulting in the absence of labeling could only be estimated when glucose was the only C source (PG). Data represent the mean of biological triplicates ± SD when appropriate. Blank data indicate the absence of growth in the tested condition (Dataset S1). M0, fraction having not integrated any ^{13}C; M + 1, fraction having integrated one ^{13}C; M57, amino acid fragments $[M-57]^+$ having conserved all C; M85 and M159, amino acid fragments $[M-85]^+$ and $[M-159]^+$ having lost the C1 during ionization.

To test this hypothesis, we compared the metabolism of seven *Brucella* strains with different preferential hosts. We found that classical zoonotic species uniquely rely on the PPP for hexose catabolism, whereas the other species utilize both the PPP and the EDP. Therefore, the latter are metabolically intermediary with soil-associated Rhizobiales using only the EDP (7–9). We demonstrated that the metabolic dichotomy among *Brucellae* emerged after the acquisition of two independent EDP-inactivating mutations in most classical zoonotic species (*B. abortus*, *B. melitensis*, and most *B. suis* biovars) as well as in *B. canis*. We then confirmed that this trait is linked to bacterial virulence in mice.

Results

Central Carbon Metabolism Functionality Discriminates Two Groups of *Brucella* Species. To test if the use of mainly the PPP represents a decisive step in the adaptation to the animal host, we compared the metabolic functionality of seven *Brucella* strains with different host preferences. Bacteria were grown in three different media of incremental complexity, i.e., Plommet medium with glucose as sole carbon source (PG), with both glucose and erythritol (PEG), and the rich medium 2× yeast extract tryptone (2YT) diluted five times and supplemented with glucose (2YT/5G). The glucose added to each medium was labeled on carbon 1 ([1-^{13}C]glucose) and used to monitor and compare the metabolism between species and media. Under growth-supporting conditions, proteinogenic amino acids from exponentially growing bacteria were extracted and their ^{13}C labeling analyzed by gas chromatography–mass spectrometry (GC/MS) (see Dataset S1 *A* and *B* for raw and processed data).

Hierarchical clustering and principal component analyses (PCAs) on the labeling data revealed the existence of two groups of *Brucella* species (Fig. 1*B* and *SI Appendix*, Fig. S1). Indeed, this clustering discriminates the strains of the classical zoonotic species (cluster I) from strains belonging to other *Brucella* species, including *B. inopinata*, which is phylogenetically closer to free-living Rhizobiales (cluster II) (14, 15).

The major difference between clusters in all tested conditions lies in the labeling profile of pyruvate-derived amino acids (see *SI Appendix* for in-depth PCAs and interpretation of isotopic-labeling data). This difference originated from distinct uses of the PPP and EDP, resulting in specific ^{13}C-incorporation patterns (Fig. 1*C*). In classical zoonotic strains (cluster I), pyruvate-derived alanine was virtually unlabeled ($[M-57]^+$ M0 = 1; Fig. 1*D*) in all tested conditions. The absence of labeling, even when glucose was the only C source, demonstrates the exclusive use of the PPP that releases ^{13}C1 as $^{13}CO_2$ (Fig. 1*C*). Conversely, a substantial proportion of alanine in species of cluster II had incorporated ^{13}C, indicating that labeled glucose has been catabolized through either glycolysis (EMP) or EDP. These two glycolytic routes yield pyruvate labeled at a different position (Fig. 1*C*), and comparisons of alanine $[M-57]^+$ (C1-C2-C3) and $[M-85]^+$ (C2-C3) fragments revealed that labeling was lost concomitantly at carbon 1. Strains from cluster II appear, therefore, to use the EDP for glucose catabolism rather than the EMP consistently with the absence of phosphofructokinase in *Brucella* species. Estimations of the percentage of pyruvate derived from [1-^{13}C]glucose catabolism via the EDP confirm that it is a major route only in strains from cluster II in all tested conditions (Fig. 1*E*). Nevertheless, the PPP seems to remain active in these strains as observed in PG.

In Vitro Growth of Key Metabolic Mutants Confirms the Metabolic Dichotomy among *Brucella* Species. To confirm our observations, we deleted the genes encoding the first enzyme specific of either the PPP (*gnd*) or the EDP (*edd*) in reference strains of *B. suis* bv. 1 (cluster I) and *B. suis* bv. 5 and *Brucella microti* (both cluster II). *B. suis* bv. 1 Δ*gnd* was unable to grow with glucose as the sole carbon source, whereas the Δ*edd* strain did not display any growth defect (Fig. 2*A*). *B. suis* bv. 1 thus exclusively catabolizes glucose through the PPP. In contrast, *gnd* deletion had respectively little or no effect on the growth of *B. suis* bv. 5 and *B. microti*. The Δ*edd* strains displayed, however, marked growth defects, thus confirming the importance of the EDP in strains of cluster II. Nevertheless, these Δ*edd* mutants were still able to grow and therefore have a functional PPP that partially compensates for the lack of EDP.

In summary, the phenotypes of key metabolic mutants confirm the observations from isotopic-labeling data and demonstrate the existence of two alternative central metabolism in *Brucella spp*. Classical zoonotic strains catabolize glucose using only the PPP, whereas those from cluster II (EDP + PPP) have a metabolism that is intermediate with soil-associated α-Proteobacteria (EDP only).

Independent Mutations in *edd* Result in EDP Inactivation in Zoonotic *Brucella* Species. We hypothesized that the metabolic shift in classical zoonotic species originated from the inactivation of Edd, the first enzyme of the EDP. Our reasoning was that 1) PPP and EDP share the first two reactions catalyzed by enzymes encoded in an operon along with *edd* in all species (Fig. 2*B* and *C*); and 2) the expression of a functional Edd along with the other genes of the operon would necessitate an active EDP to prevent the toxic accumulation of the intermediate metabolite 2-keto-3-deoxy-6-phosphogluconate (16).

To investigate this hypothesis, we compared the *edd* sequence of *Brucella* species and other α-Proteobacteria for which the use of EDP has been experimentally demonstrated. This analysis revealed the insertion of a seventh adenine within a stretch of six that creates a frameshift (S407fs) in *B. suis* bv. 1 *edd* compared with all of the other species. This insertion modifies 25% of the Edd protein sequence on its carboxy (C)-terminal end (Fig. 2*D*). To test the impact of the mutation, we tried to suppress *B. suis* bv. 5 Δ*edd* growth defect in PG by complementing with either the endogenous gene or with a frameshifted copy from *B. suis* bv. 1 (Fig. 2*E*). Only the endogenous gene restored wild-type (WT) growth, proving that the S407fs causes the loss of Edd function. This frameshift is conserved in all sequenced *B. suis* strains (bv. 1, 2, and 3; $n = 97$) as well as in the related *B. canis* but not in *B. suis* bv. 4.

In all *B. abortus* and *B. melitensis* sequenced, we identified a conserved nonsynonymous mutation A178P (Fig. 2*D*). This substitution introduces a proline in a β-strand predicted to be deeply buried into the protein, likely resulting in enzyme inactivation. Transcomplementation of *B. suis* bv. 5 Δ*edd* with *B. abortus edd*^{A178P} and the reverted *edd*^{P178A} showed that only the latter restored growth on glucose (Fig. 2*F*). These results confirm that the A178P mutation is responsible for Edd dysfunction and thus for EDP inactivation in *B. abortus* and *B. melitensis*.

In summary, the exclusive use of the PPP observed in *Brucella* strains from cluster I is consecutive to two independent mutations inactivating Edd (S407fs and A178P), resulting in a nonfunctional EDP in *B. abortus*, *B. melitensis*, *B. canis*, and *B. suis* bv. 1, 2, and 3. As these inactivation events occurred independently in different species, our finding supports that there was a convergent evolution toward the exclusive use of the PPP in these bacteria.

These observations further indicated that our *B. suis* bv. 1 Δ*gnd*, being a natural *edd* mutant, had both EDP and PPP pathways inactivated. This is surprising since without Gnd, a functional Edd and a Pfk for the otherwise interrupted EMP, there is no known pathway left for hexose catabolism. It raises the hypothesis of an unknown distinct metabolism or that compensatory mutations might have paralleled the loss of a functional *edd* in this strain. Nevertheless, the deletion of *gnd* in *B. suis* bv. 1 is not insignificant since it results in a marked growth defect even in rich medium (*SI Appendix*, Fig. S2). We tried to reproduce this genotype in *B. suis* bv. 5 by doing a second round of homologous recombination to delete *gnd* in the Δ*edd* strain or *edd* in the Δ*gnd* background. No

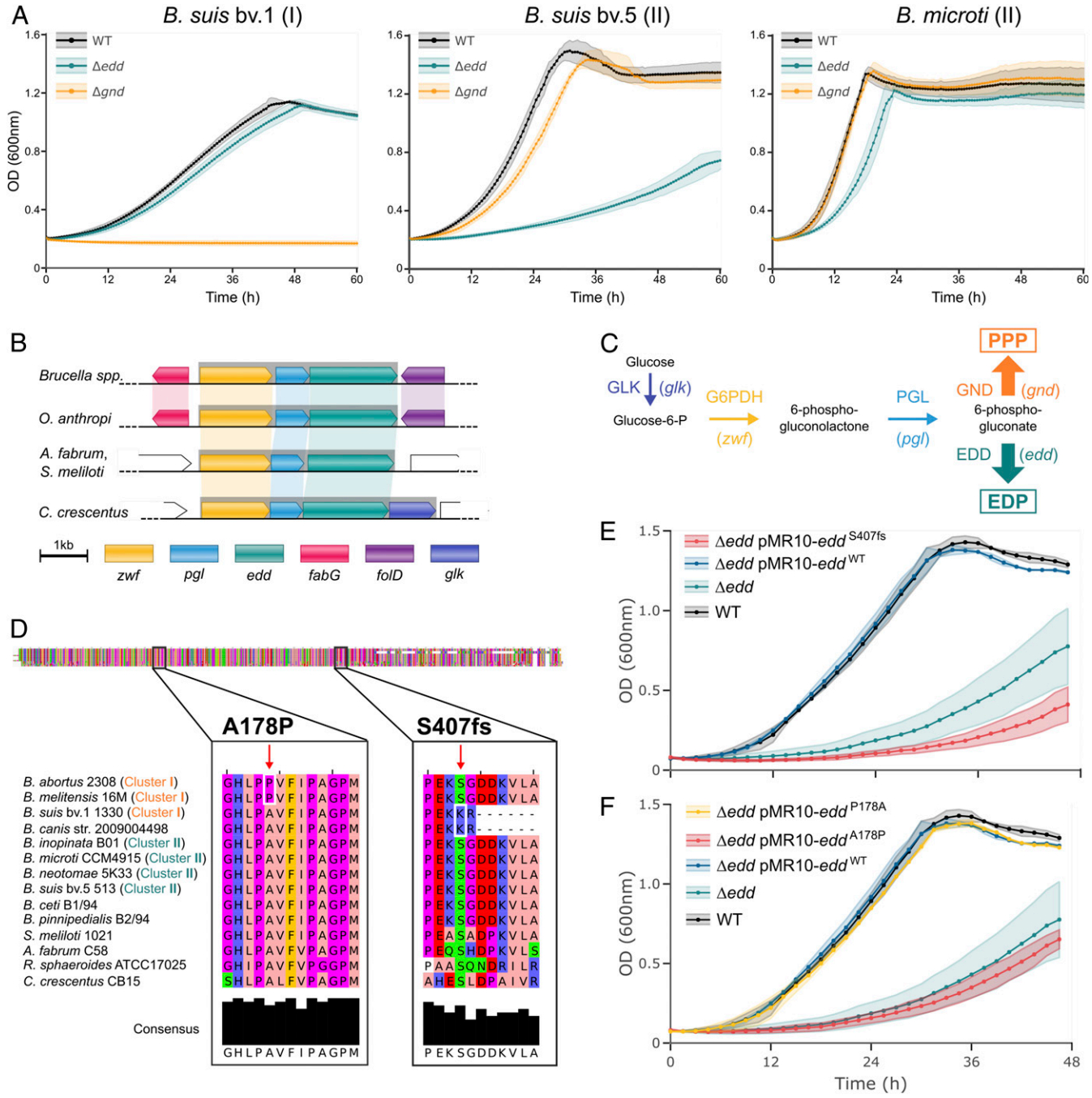

Fig. 2. The metabolic switch of zoonotic *Brucella* species is due to Edd inactivation. (*A*) Growth on glucose of key metabolic mutants devoid of the EDP (Δ*edd*) or the PPP (Δ*gnd*) with glucose. (*B* and *C*) Genes required for glucose catabolism through both PPP and EDP (*zwf* and *pgl*) are organized in a conserved operon (gray) with *edd*. (*D*) Edd protein sequence comparisons highlighted the presence of a nonsynonymous mutation (A178P) conserved in *B. abortus* 2308 and *B. melitensis* 16M as well as a frameshift (S407fs) in *B. suis* bv. 1 and *B. canis*. *A. fabrum*, *Agrobacterium fabrum*; *B. ceti*, *Brucella ceti*; *B. pinnipedialis*, *Brucella pinnipedialis*. (*E* and *F*) Complementation of *B. suis* bv. 5 Δ*edd* growth defect in PG with the endogenous gene (pMR10-*edd*^{WT}), the frame-shifted gene from *B. suis* bv. 1 (pMR10-*edd*^{S407fs}), the A178P mutated gene from *B. abortus* 2308 (pMR10-*edd*^{A178P}) or the same gene with a reverted mutation (pMR10-*edd*^{P178A}). Data represent the mean ± SD (shaded area) of biological duplicates.

double mutant could be obtained, demonstrating that these two deletions are synthetic lethal in *B. suis* bv. 5 ($P < 10^{-15}$ to delete *gnd* and $P < 3.10^{-5}$ to delete *edd* with a χ^2 analysis assuming an expected 50:50 distribution of WT and Δ genotypes post-recombination). This synthetic lethality observed in *B. suis* bv. 5 being not conserved in *B. suis* bv. 1 highlights the existence of other interspecies metabolic differences. The existence of such differences is also supported by the strain-specific capability to grow on the different media tested (Fig. 1*B*) and will need to be further investigated.

The Exclusive Use of the PPP Alters the Outcome of *B. Microti* Infection in BALB/C Mice. We hypothesized that the selection of the PPP might indicate a selective advantage conferred in the context of infection. Since it is virtually impossible to experimentally test the virulence of our mutant strains in their native host, or to evaluate

their zoonotic potential, we resorted to the mouse model of infection. Typically, classical zoonotic brucellae are pathogens capable of setting sustained intracellular infections in natural hosts that can be reproduced in the mouse model. In contrast, the same doses of *B. microti* result in rapid clearance or lethality (17). Therefore, there are three classes of *Brucella* at the intersection of metabolism and virulence, those that use only the PPP (e.g., *B. suis* bv. 1), those that use mostly the EDP (e.g., *B. suis* bv. 5) and cause sustained infections, and those that use mostly the EDP and are comparatively unable to persist (e.g., *B. microti*). We explored the hypothetical link between hexose metabolism and virulence in mice in a representative strain of each of these three classes. Specifically, BALB/c mice were infected by WT, Δ*gnd*, and Δ*edd* strains of *B. suis* bv. 1, *B. suis* bv. 5, and *B. microti*. As expected, the deletion of the nonfunctional *edd* in *B. suis* bv. 1 did not affect the number of colony-forming units (CFUs), whereas the Δ*gnd* mutant was significantly attenuated (Fig. 3*A*). These results demonstrate the importance of hexose metabolism and of the PPP in vivo in *Brucella* spp. belonging to cluster I. In *B. suis* bv. 5, the loss of either *gnd* (PPP) or *edd* (EDP) had no impact on the infection (Fig. 3*B*). In contrast, despite similar CFU numbers between *B. microti* WT, Δ*edd*, and Δ*gnd* strains in the spleen (Fig. 3*C*), the host survival kinetic was significantly modified dependent on metabolism (Fig. 3*D*). The Δ*edd* mutant relying only the PPP, like classical zoonotic species, killed mice more rapidly and led to a lower survival rate than the parental strain (Fig. 3*D*). The Δ*gnd* mutant turned out to have the opposite phenotype, being innocuous.

The disconnection between unmodified CFU counts and host survival in *B. microti* indicates an altered immunogenicity in the mutants rather than a difference in terms of replication. These results demonstrate a direct but subtle link between the metabolic switch described here and virulence in *Brucella*. Classical zoonotic species have lost metabolic plasticity, which, similarly to genome reduction, might represent a feature of pathogen specialization (10, 12). Then, the impact of *B. microti* metabolism on host survival supports that the downstream effects of the metabolic switch impact the host–pathogen interaction. The difference observed between *B. microti* and *B. suis* bv. 5 infection indicates, however, that this impact might be moderate as only observable when the infection is lethal. This difference might also indicate that other factors could be involved, such as subtle qualitative and/or quantitative differences in the pathogen-associated molecular patterns (PAMPs) that are known to be critical for *Brucella* persistence in the host (18). If so, the selection of the PPP over the EDP would postdate other adaptation mechanisms allowing induction of sustained infections, resulting otherwise in excessive host death. *B. microti* and then *B. suis* bv. 5 might thus be representative of intermediate evolutionary steps between EDP-dependent free-living α-Proteobacteria and PPP-dependent zoonotic *Brucella* species.

Discussion

The red queen hypothesis posits that hosts and pathogens are running a never-ending arms race imposing reciprocal selective pressures (19). Each host might consequently impose unique constraints on a pathogen that, in turn, might follow similarly unique evolutionary trajectories. We here more specifically studied how bacterial metabolism has been adjusted relative to different hosts by comparing the metabolic functionality of multiple *Brucella* species scattered across their phylogenetic tree and with different host preferences. We identified two main metabolic classes of *Brucella*, species closer to soil-associated α-Proteobacteria that use both EDP and PPP, and those that have evolved in contact with domestic animals or their ancestors that rely only on a functional PPP. Based on these observations, we propose a model of stepwise central carbon-metabolism evolution in *Brucella* species. It starts with the ancestor to all *Brucellae* being a free-living soil bacterium (6) whose hexose catabolism was likely exclusively relying on the EDP. This feature is conserved among other phylogenetically close α-Proteobacteria living in soil (e.g., *Agrobacterium tumefaciens* and *Sinorhizobium meliloti*) (8), freshwaters (e.g., *Caulobacter crescentus*

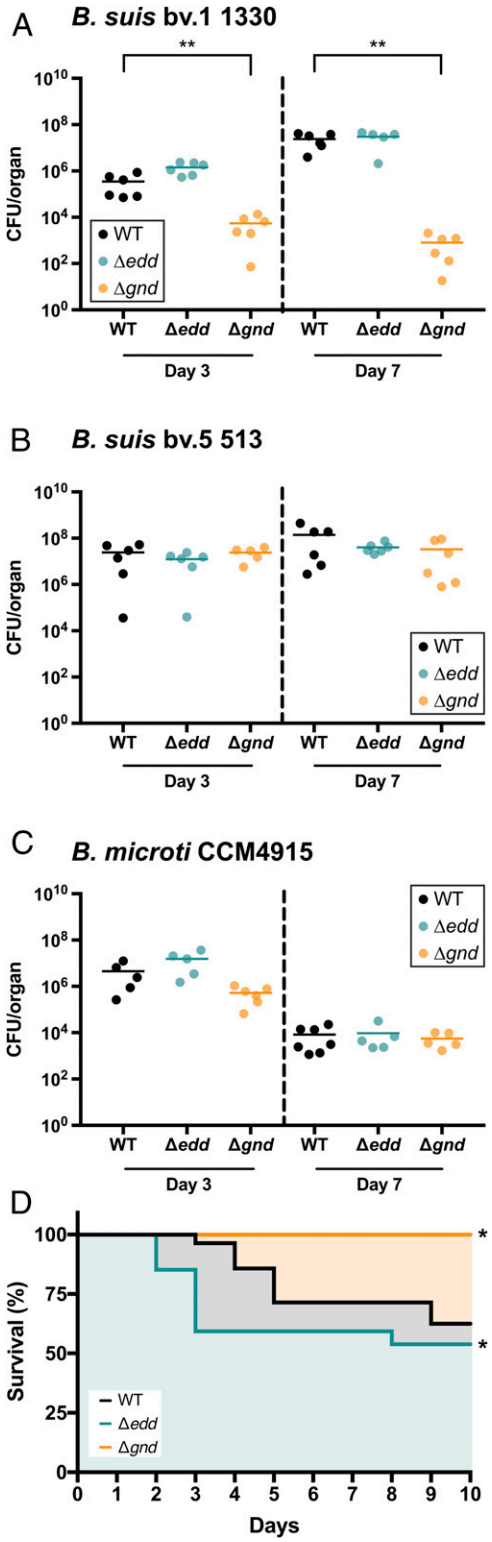

Fig. 3. Consequences of the metabolic switch during the intraperitoneal infection of BALB/c mice. (*A–C*) Average splenic CFUs enumerated 3 and 7 d postinfection with *B. suis* bv. 1 (*A*), *B. suis* bv. 5 (*B*), and *B. microti* (*C*). (*D*) Survival kinetics of mice infected with *B. microti*. *$P < 0.05$; **$P < 0.01$.

and *Rhodobacter sphaeroides*) (8, 13), or marine environments (e.g., *Dinoroseobacter shibae* and *Phaeobacter gallaeciensis*) (20). All of these environments are oligotrophic and therefore favor the EDP over the EMP or PPP because of its higher thermodynamic driving force and reduced need for energy-costly enzymes to achieve the same glucose conversion (21). Such a *Brucella* ancestor would have then transitioned to a facultative intracellular lifestyle and metabolically diverged by using both EDP and PPP. This property is common to the most *Brucella* strains in cluster II, as described here. At this stage, the ancestor might have also transitioned from a poorly adapted pathogen like *B. microti* to a bacterium capable of inducing sustained infections following a path including, notably, a reduction of PAMPs, as proposed before (18). Later, the common ancestor of *B. abortus* and *B. melitensis*, as well as the ancestor of *B. suis* bv. 1, 2, and 3 (and therefore of *B. canis*), would have independently acquired EDP-inactivating mutations (*edd* A178P and S407fs, respectively). These mutations would finally account for the PPP-exclusive metabolism described here in cluster I brucellae. An exception within cluster I lineages is *B. suis* bv. 4, which seems to possess a functional EDP based on *edd* and *eda* sequences. One hypothesis is that the mutations have not taken place yet in this strain because of a relatively short time of evolution in association with reindeers, its preferential host. Considering the explosive irradiation of core brucellae (6), we favor this hypothesis over the possibility that there might exist host specificities that conditioned the evolution of the pathogen.

Interestingly, the selection of the PPP over the EDP in pathogenic bacteria described here does not seem to be restricted to *Brucella* as it seems to have also occurred in mycobacteria. The nonpathogenic, soil-living *Mycobacterium smegmatis* was initially described as possessing both functional EDP and PPP pathways (22). Interestingly, we observed that in *M. smegmatis*, each pathway is genetically encoded in dedicated operons, *zwf-edd-eda* for the EDP and *zwf-pgl-tkt-tal* for the PPP. While the PPP-associated operon is conserved, pathogenic mycobacteria capable of inducing sustained infections, such as *Mycobacterium tuberculosis*, have lost the EDP operon. Consistently, the loss of the EDP operon provides a genetic rationale for the absence of EDP activity detectable in another pathogen, *Mycobacterium leprae* (23). These coincidences support the hypothesis of the existence of an evolutionary trajectory bridging the loss of the EDP and bacterial virulence that has been adopted by at least some important intracellular bacterial pathogens.

The rationale for the selection of the PPP over the EDP at the expense of metabolic plasticity could rely on differences in enzyme robustness. The iron–sulfur cluster-containing Edd is sensitive to both iron scarcity and reactive oxygen species, two stresses encountered in host macrophages, rendering the EDP less amenable for the infection context (24–26). A second, nonexclusive, explanation for the selection of the PPP is the difference in yields existing between the two pathways. The absence of Pfk in *Brucella* imposes that the PPP works as a cycle (cPPP) (*SI Appendix*, Fig. S3) (1). Assuming 1) a purely catabolic purpose with pyruvate as end product, 2) an NADP-dependent glucose-6-phosphate (glucose-6-P) dehydrogenase, and 3) an NAD-dependent 6-phosphogluconate dehydrogenase (27, 28), the cPPP would yield three times more NADPH than the EDP. In the context of infection, higher NADPH availability may be advantageous to cope with oxidative stress. Consistently, while mycobacteria accumulate glucose-6-P in normal growth conditions, the pool is depleted in oxidative-stress conditions and has to be metabolized through the PPP for optimal survival (29).

Another advantage of a PPP-specific metabolism might be an increase in biomass precursor availability along with NADPH that also drives anabolic reductions. The cPPP produces 5 out of 12 biomass precursors required, for instance, to synthesize aromatic amino acids such as tryptophan. It would notably allow countering the indoleamine 2,3-dioxygenase–dependent tryptophan depletion observed in IFN-γ–activated macrophages, a strategy also adopted by *Listeria monocytogenes* (30, 31).

In summary, the existence of a metabolic dichotomy among brucellae indicates that a progressive metabolic transition has occurred during the evolution of the classical zoonotic species. Our hypothesis is that they have transitioned from an EDP-based metabolism to using both EDP and PPP before conserving only the PPP in fine. Remarkably, the PPP has been selected at least twice during *Brucella* history and originates from the acquisition of EDP-inactivating mutations. This argues for a link between a PPP-based metabolism and the characteristic ability of classical zoonotic species to cause sustained infections, which is substantiated by our mouse infection data. The latter data furthermore indicate that the consequences of losing the EDP might be subtle and would postdate other traits associated with the ability to establish their characteristic type of infection. This evolutionary trajectory might also have occurred in intracellular pathogens, as in *M. tuberculosis* or *M. leprae*. Finally, our results illustrate that reshaping metabolism is crucial in host colonization by pathogens. Moreover, we only focused on a single, major metabolic adaptation, but there are many more to unveil as each of the tested *Brucella* species appeared to have a unique metabolic signature.

Material and Methods

Bacterial Cultures and Growth Measurements. The *Brucella* species used were *B. melitensis* 16M, *B. abortus* 2308, *B. suis* bv. 1 str. 1330, *B. suis* bv. 5 str. 513, *B. microti* CCM4915, *Brucella neotomae* 5K33, and *B. inopinata* B01. They were grown at 37 °C in rich-medium 2YT (16 g/L Bactotryptone; 10 g/L yeast extract; 5 g/L NaCl; Difco) or in a chemically defined medium adapted from Plommet medium (32, 33) composed of 2.3 g/L K_2HPO_4, 3 g/L KH_2PO_4, 0.1 g/L $Na_2S_2O_3$, 5 g/L NaCl, 0.2 g/L nicotinic acid, 0.2 g/L thiamine, 0.07 g/L pantothenic acid, 0.5 g/L $(NH_4)_2SO_4$, 0.01 g/L $MgSO_4$, 0.1 mg/L $MnSO_4$, 0.1 mg/L $FeSO_4$, 0.1 mg/L biotin and supplemented with a defined C source (addition of methionine 1 mM is needed for the growth of *B. melitensis* 16M in Plommet medium). Chloramphenicol (20 μg/mL), kanamycin (Kan) (50 μg/mL), polymyxin B (2 μg/mL), sucrose (5% wt/vol), and agar were added when required. Cultures in the chemically defined medium were performed in three steps: 1) 24 h of culture in 2YT; 2) dilution to an optical density (OD) of 0.1 in the chemically defined medium and incubation for 16 h; and 3) dilution to an OD of 0.1 in the defined medium after centrifugation and removal of the supernatant.

For isotopic-labeling experiments, 2YT/5G was prepared by diluting five times 2YT with distilled water and adding 2 g/L [1-^{13}C]glucose (Cortecnet), and PEG was prepared by supplementing modified Plommet with 1 g/L [U-^{12}C]erythritol and 2 g/L [1-^{13}C]glucose, whereas PG was prepared by only adding labeled glucose at the same concentration.

Growth kinetics experiments were performed by monitoring the OD (600 nm) during 48 to 96 h in an automated plate reader (Bioscreen C; Lab Systems) with continuous shaking at 37 °C.

Proteinogenic Amino Acid Extraction and GC/MS Analysis. Bacteria were grown in 2YT/5G, PEG, and PG in Erlenmeyer flasks. Volumes corresponding to at least 1 mg of bacterial dry weight (DW) were sampled mid-log phase (OD_{600}: ~0.4) and stored at −80 °C until extraction. Pellets were washed twice with an isosmotic solution of NaCl and hydrolyzed at 105 °C for 22 h with 50 μL/mg DW of HCl 6N. Cell debris were removed by filtration (Ultrafree-MC Centrifugal Filter Devices; Amicon) before lyophilization. Prior to measurement, hydrolysates were dried under a nitrogen stream, and amino acids were turned into their *t*-butyl-di-methyl-silyl derivates by incubation at 80 °C for 30 min with 50 μL of *N*-methyl-*N*-tert-butyldimethylsilyl-trifluoroacetamide and 50 μL of 0.1% pyridine in dimethylformamide (34). Derivatized samples were then injected into a GC/MS system for labeling-pattern determination (Agilent 7890A and MSD 5979C; Agilent Technologies). Amino acid separation was performed using an Agilent HP5MS capillary column (5% phenyl-methyl-siloxane diphenylpolysiloxane; 30 m × 250 μm) with 1 mL·min^{-1} helium as a carrier gas and the following temperature profile: 120 °C for 2 min, 8 °C·min^{-1} up to 200 °C, and 10 °C·min^{-1} until 325 °C is reached. Finally, amino acids were ionized by electron ionization (70 eV), fragmented, and detected using a triple-quadrupole detector with inlet, interface, and quadrupole temperatures set at 250, 280, and 230 °C, respectively. Each labeling analysis comprised one measurement in scan mode to check for isobaric-fragment overlays. Relative fractions of relevant mass

isotopomers were then determined in duplicate in selective ion monitoring mode. Isotopomers [M-57] and [M-85] were the most used as they include all carbons and all carbons but the first, respectively (35, 36). Steady-state labeling pattern was therefore calculated as mean value of 18 measurements for every investigated conditions (3 biological replicates, 3 samples, 2 technical duplicates). Data were then corrected for naturally occurring isotopes as well as for the inoculum using IsoCor (37).

Glycolytic fluxes estimation. [1-^{13}C]Glucose catabolism via the three glycolytic routes (EMP/PPP/EDP) results in distinct triosephosphate-labeling patterns (Fig. 1 *C* and *D*). This difference allows quantification of the contribution of each pathway for glucose breakdown.

In PG, glycolytic fluxes were estimated similarly as previously described (20, 38). In brief, we estimated PPP contribution (%*PPP*) by comparing experimental (*exp*) and theoretical (*th*) labeling patterns of alanine [M-57]$^+$, whereas glycolysis contribution (%*EMP*) was based on serine [M-85]$^+$ fragment. We finally evaluated EDP contribution (%*EDP*) by subtracting %*EMP* and %*PPP* from total activity:

$$\%PPP = \frac{Ala[M-57] + M0exp - Ala[M-57] + M0EDP/EMPth}{Ala[M-57] + M0PPPth - Ala[M-57] + M0EDP/EMPth} = \frac{Ala[M-57] + M0exp - 0.5}{0.5} \times 100$$

$$\%EMP = \frac{Ser[M-85] + M0exp - Ser[M-85] + M0EDP/PPPth}{Ser[M-85] + M0EMPth - Ser[M-85] + M0EDP/PPPth} = \frac{Ser[M-85] + M0exp - 1}{-0.5} \times 100$$

$$\%EDP = 100 - \%PPP - \%EMP.$$

For the conditions involving a mix of unlabeled substrates and [1-^{13}C]glucose (PEG, 2YT/5G), it is impossible to estimate the %*PPP*. Indeed, the lack of ^{13}C incorporation could result indiscriminately from either [1-^{13}C]glucose catabolism via the PPP or the metabolism of the additional C sources. Similarly, since the %*EDP* was directly calculated from the %*PPP* (equation), it could not be estimated as previously. Instead, we used the percentage of C3 compounds having acquired a ^{13}C on C1 and C3 as a metric for EDP and EMP activities, respectively. Since it is reasonable to assume that only 50% of the C3 compounds produced by both pathways are labeled, we multiplied these percentages by 2:

$$\%EMP = Ser[M-85] + M+1exp \times 2 \times 100$$

$$\%EDP = Ala[M-57] + M+1exp - Ala[M-85] + M+1exp \times 2 \times 100.$$

Both estimation methods yielded highly similar values in PG with a correlation coefficient $R2 > 0.99$ supporting their consistency. Since estimations in PEG and 2YT/5G quantify the percentage of [1-^{13}C]glucose-derived C3 compounds and do not take into account the contribution of the unlabeled substrate(s), obtained percentages are lower than in PG with %*EMP* + %*PPP* + %*EDP* <100.

Bioinformatics and Data Analyses. Hierarchical clustering was performed on all isotopic-labeling data (mean of biological triplicates for each fragment; Fig. 1*B*) using Euclidean distances and Ward's method. To further characterize intercluster metabolic differences, PCAs were carried out on centered unscaled labeling data individually for each tested medium (*SI Appendix*) using FactoMineR and Factoextra (39).

For Edd protein sequence comparisons, sequences from multiple *Brucella* species along with other phylogenetically close α-Proteobacteria were aligned using MUltiple Sequence Comparison by Log-Expectation (MUSCLE) (40) and visualized using Jalview (41).

Construction of Deletion and Complementation Strains. The locus tag identifiers and nucleotide sequences of the genes *edd*, *eda*, and *gnd* for *B. abortus* 2308, *B. melitensis* 16M, *B. suis* bv. 1 1330, and *B. suis* bv. 5 str. 513 are provided in Dataset S2. Construction of in-frame clean-deletion strains Δ*edd* (BAB2_0458) and Δ*gnd* (BAB2_0109) in *Brucella* species was done similarly as previously described (32, 42). Briefly, sequences of 750 base pairs upstream (up) and downstream (dw) the gene to delete were amplified by PCR using the Phusion high-fidelity DNA polymerase (ThermoScientific) from genomic DNA (see Dataset S3 for primer sequences). The two PCR products were then separately ligated in an intermediate pGEM Easy plasmid digested with *Eco*RV (Promega). Insert sequences were checked by sequencing (Beckman Coulter Genomics) before excision and ligation of up and dw fragments in an appropriately digested pNPTS138 suicide vector (Kan^R Suc^S). The latter vector was introduced in *Brucella* species by conjugation with the S17-1 *Escherichia coli* donor strain. We selected vector insertion events with kanamycin along with either nalidixic acid or polymyxin B to counter select the *E. coli* donor strain. Plasmid excision was then selected using sucrose sensitivity conferred by the *sacB* gene along with the loss of kanamycin resistance. Gene deletion was finally checked by PCR using at least one primer external to the construction.

For complementation constructs, deleted genes were PCR-amplified using one pair of primers (Dataset S3) on the genomic DNA of different *Brucella* species. We sequenced the amplicons before ligation as *Xho*I-*Bam*HI inserts in the low-copy episomal vector pMR10 (Kan^R). To revert the inactivated A178P Edd to a functional protein (P178A), we built a complementation vector after introducing a single point mutation. To do so, *edd* from *B. abortus* 2308 was PCR-amplified as two partially overlapping PCR products (edd_comp_f/edd_comp_P178A_r2 and edd_comp_P178A_f2/edd_comp_r) with the corrective mutation in the floating end of primer f2. Both PCR products were assembled during a third PCR using primers edd_comp_f and edd_comp_r. We then sequenced the product before ligating it as an *Xho*I-*Bam*HI insert in the pMR10 vector.

BALB/c Mice Infection. We performed the procedures and handling of mice in an Animal Biosafety Level 3 facility in compliance with current European legislation (directive 86/609/EEC) and the corresponding Belgian law "Arrêté royal relatif à la protection des animaux d'expérience du 6 avril 2010 publié le 14 mai 2010." The Animal Welfare Committee of the Université de Namur (Belgium) reviewed and approved the complete protocols (Permit 05-058 LE).

Female BALB/c mice (8 to 12 wk old) were intraperitoneally infected as previously described (43). In brief, bacteria from an overnight culture in 2YT were pelleted, washed with Roswell Park Memorial Institute Medium 1640, and diluted in this medium. We injected 500 μL of suspension (10^5 CFUs) into groups of at least six mice for each tested strain.

For CFU counting, mice were euthanized by cervical dislocation and CO_2 euthanasia during the acute phase of infection, i.e., 3 and 7 d postinjection. Spleens were isolated and homogenized in 1 mL of 1x phosphate-buffered saline/0.1% Triton X-100. Homogenates were then serially diluted and plated on tryptic soy agar plates. The Mann–Whitney *U* test was used to identify significant differences in CFU counts.

Survival kinetics upon infection by *B. microti* strains were conducted similarly as described previously (17). Animals' well-being was followed twice a day after infection for signs of distress and end points such as impaired motility, labored breathing, ruffled hair coat, hunching, prostration, dehydration, and weight loss. Mice exhibiting multiple criteria with severe symptoms were euthanized as previously described and were considered nonsurvivors. The Gehan–Breslow–Wilcoxon test was used to highlight significant differences in host survival kinetics.

Data Availability. All study data are included in the article and *SI Appendix*.

ACKNOWLEDGMENTS. The University of Namur provided financial and logistical support. This work was funded by the Fonds de la Recherche Scientifique (FRS-FNRS) "Brucell-cycle" grant (PDR T.0060.15). A.M. was supported by a Fonds pour la Formation à la Recherche dans l'Industrie et dans l'Agriculture (FRIA) PhD fellowship from FRS-FNRS. T.B. held an Aspirant Fellowship from FRS-FNRS. Research at the "Universidad de Navarra" was supported by the Institute of Tropical Health (ISTUN) funders (Obra Social la Caixa [LCF/PR/PR13/11080005] and Fundación Caja Navarra, Fundación María Francisca de Roviralta, Ubesol, and Inversiones Garcilaso de la Vega SL). We thank Raquel Conde-Álvarez and Michael Chao for critical reading of this manuscript.

1. J. Batut, S. G. E. Andersson, D. O'Callaghan, The evolution of chronic infection strategies in the α-proteobacteria. *Nat. Rev. Microbiol.* **2**, 933–945 (2004).
2. J. Godfroid *et al*., From the discovery of the Malta fever's agent to the discovery of a marine mammal reservoir, brucellosis has continuously been a re-emerging zoonosis. *Vet. Res.* **36**, 313–326 (2005).
3. J. Godfroid *et al*., Brucellosis at the animal/ecosystem/human interface at the beginning of the 21st century. *Prev. Vet. Med.* **102**, 118–131 (2011).
4. M. Suárez-Esquivel *et al*., Brucella neotomae infection in humans, Costa Rica. *Emerg. Infect. Dis.* **23**, 997–1000 (2017).
5. E. Moreno, I. Moriyón, "The genus Brucella" in *The Prokaryotes*, M. Dworkin, S. Falkow, E. Rosenberg, K. H. Schleifer, E. Stackebrandt, Eds. (Springer, New York, 2006), pp. 315–456.
6. A. R. Wattam *et al*., Comparative phylogenomics and evolution of the Brucellae reveal a path to virulence. *J. Bacteriol.* **196**, 920–930 (2014).

7. T. Barbier *et al*., Brucella central carbon metabolism: An update. *Crit. Rev. Microbiol.* **44**, 182–211 (2018).
8. T. Fuhrer, E. Fischer, U. Sauer, Experimental identification and quantification of glucose metabolism in seven bacterial species. *J. Bacteriol.* **187**, 1581–1590 (2005).
9. M. D. Stowers, Carbon metabolism in Rhizobium species. *Annu. Rev. Microbiol.* **39**, 89–108 (1985).
10. R. C. Essenberg, R. Seshadri, K. Nelson, I. Paulsen, Sugar metabolism by Brucellae. *Vet. Microbiol.* **90**, 249–261 (2002).
11. D. C. Robertson, W. G. McCullough, The glucose catabolism of the genus Brucella. I. Evaluation of pathways. *Arch. Biochem. Biophys.* **127**, 263–273 (1968).
12. D. C. Robertson, W. G. McCullough, The glucose catabolism of the genus Brucella. II. Cell-free studies with B. abortus (S-19). *Arch. Biochem. Biophys.* **127**, 445–456 (1968).
13. R. G. Riley, B. J. Kolodziej, Pathway of glucose catabolism in Caulobacter crescentus. *Microbios* **16**, 219–226 (1976).
14. E. Moreno, Genome evolution within the alpha proteobacteria: Why do some bacteria not possess plasmids and others exhibit more than one different chromosome? *FEMS Microbiol. Rev.* **22**, 255–275 (1998).
15. P. S. G. Chain *et al*., Whole-genome analyses of speciation events in pathogenic Brucellae. *Infect. Immun.* **73**, 8353–8361 (2005).
16. P. Allenza, T. G. Lessie, Pseudomonas cepacia mutants blocked in the Entner-Doudoroff pathway. *J. Bacteriol.* **150**, 1340–1347 (1982).
17. M. P. Jiménez de Bagüés *et al*., The new species Brucella microti replicates in macrophages and causes death in murine models of infection. *J. Infect. Dis.* **202**, 3–10 (2010).
18. A. Martirosyan, E. Moreno, J.-P. Gorvel, An evolutionary strategy for a stealthy intracellular Brucella pathogen. *Immunol. Rev.* **240**, 211–234 (2011).
19. L. V. Valen, A new evolutionary law. *Evol. Theory* **1**, 1–30 (1973).
20. T. Fürch *et al*., Metabolic fluxes in the central carbon metabolism of Dinoroseobacter shibae and Phaeobacter gallaeciensis, two members of the marine Roseobacter clade. *BMC Microbiol.* **9**, 209 (2009).
21. A. Flamholz, E. Noor, A. Bar-Even, W. Liebermeister, R. Milo, Glycolytic strategy as a tradeoff between energy yield and protein cost. *Proc. Natl. Acad. Sci. U.S.A.* **110**, 10039–10044 (2013).
22. N. J. Bai, M. R. Pai, P. S. Murthy, T. A. Venkitasubramanian, Pathways of glucose catabolism in Mycobacterium smegmatis. *Can. J. Microbiol.* **22**, 1374–1380 (1976).
23. P. R. Wheeler, Catabolic pathways for glucose, glycerol and 6-phosphogluconate in Mycobacterium leprae grown in armadillo tissues. *J. Gen. Microbiol.* **129**, 1481–1495 (1983).
24. P. R. Gardner, I. Fridovich, Superoxide sensitivity of the Escherichia coli 6-phosphogluconate dehydratase. *J. Biol. Chem.* **266**, 1478–1483 (1991).
25. S. S. Sasnow, H. Wei, L. Aristilde, Bypasses in intracellular glucose metabolism in iron-limited Pseudomonas putida. *MicrobiologyOpen* **5**, 3–20 (2016).
26. M. Rodriguez, A. G. Wedd, R. K. Scopes, 6-phosphogluconate dehydratase from Zymomonas mobilis: An iron-sulfur-manganese enzyme. *Biochem. Mol. Biol. Int.* **38**, 783–789 (1996).
27. T. Fuhrer, U. Sauer, Different biochemical mechanisms ensure network-wide balancing of reducing equivalents in microbial metabolism. *J. Bacteriol.* **191**, 2112–2121 (2009).
28. F. Sosa-Saavedra, M. León-Barrios, R. Pérez-Galdona, Pentose phosphate pathway as the main route for hexose catabolism in Bradyrhizobium sp. lacking Entner–Doudoroff pathway. A role for NAD+-dependent 6-phosphogluconate dehydrogenase (decarboxylating). *Soil Biol. Biochem.* **33**, 339–343 (2001).
29. M. R. Hasan, M. Rahman, S. Jaques, E. Purwantini, L. Daniels, Glucose 6-phosphate accumulation in mycobacteria: Implications for a novel F420-dependent anti-oxidant defense system. *J. Biol. Chem.* **285**, 19135–19144 (2010).
30. W. Däubener, C. R. MacKenzie, "IFN-gamma activated indoleamine 2,3-dioxygenase activity in human cells is an antiparasitic and an antibacterial effector mechanism" in *Tryptophan, Serotonin, and Melatonin*, G. Huether , Eds. (Springer, 1999), pp. 517–524.
31. S. V. Schmidt, J. L. Schultze, New insights into IDO biology in bacterial and viral Infections. *Front. Immunol.* **5**, 384 (2014).
32. T. Barbier *et al*., Erythritol feeds the pentose phosphate pathway via three new isomerases leading to D-erythrose-4-phosphate in Brucella. *Proc. Natl. Acad. Sci. U.S.A.* **111**, 17815–17820 (2014).
33. M. Plommet, Minimal requirements for growth of Brucella suis and other Brucella species. *Zentralbl. Bakteriol.* **275**, 436–450 (1991).
34. C. Wittmann, M. Hans, E. Heinzle, In vivo analysis of intracellular amino acid labelings by GC/MS. *Anal. Biochem.* **307**, 379–382 (2002).
35. P. Millard, F. Letisse, S. Sokol, J.-C. Portais, Correction of MS data for naturally occurring isotopes in isotope labelling experiments. *Methods Mol. Biol.* **1191**, 197–207 (2014).
36. C. Wittmann, Fluxome analysis using GC-MS. *Microb. Cell Fact.* **6**, 6 (2007).
37. P. Millard, F. Letisse, S. Sokol, J.-C. Portais, IsoCor: Correcting MS data in isotope labeling experiments. *Bioinformatics* **28**, 1294–1296 (2012).
38. A. Klingner *et al*., Large-Scale 13C flux profiling reveals conservation of the Entner-Doudoroff pathway as a glycolytic strategy among marine bacteria that use glucose. *Appl. Environ. Microbiol.* **81**, 2408–2422 (2015).
39. S. Lê, J. Josse, F. Husson, FactoMineR: An RPackage for multivariate analysis. *J. Stat. Softw.* **25**, 1–18 (2008).
40. R. C. Edgar, MUSCLE: Multiple sequence alignment with high accuracy and high throughput. *Nucleic Acids Res.* **32**, 1792–1797 (2004).
41. A. M. Waterhouse, J. B. Procter, D. M. A. Martin, M. Clamp, G. J. Barton, Jalview Version 2–A multiple sequence alignment editor and analysis workbench. *Bioinformatics* **25**, 1189–1191 (2009).
42. A. Zúñiga-Ripa *et al*., Brucella abortus depends on pyruvate phosphate dikinase and malic enzyme but not on Fbp and GlpX fructose-1,6-bisphosphatases for full virulence in laboratory models. *J. Bacteriol.* **196**, 3045–3057 (2014).
43. R. Copin *et al*., In situ microscopy analysis reveals local innate immune response developed around Brucella infected cells in resistant and susceptible mice. *PLoS Pathog.* **8**, e1002575 (2012).